

Cytotoxicity and cell membrane depolarization induced by aluminum oxide nanoparticles in human lung epithelial cells A549

Weisheng Lin^a, Isaac Stayton^a, Yue-wern Huang^b, Xiao-Dong Zhou^c
and Yinfa Ma^{a*}

^aDepartment of Chemistry and Environmental Research Center, University of Missouri-Rolla, Rolla, Missouri, USA; ^bDepartment of Biological Sciences and Environmental Research Center, University of Missouri-Rolla, Rolla, Missouri, USA; ^cPacific Northwest National Laboratory, Richland, Washington, USA

(Received 6 June 2007; final version received 8 November 2007)

The cytotoxicity of 13 and 22 nm aluminum oxide (Al₂O₃) nanoparticles was investigated in cultured human bronchoalveolar carcinoma-derived cells (A549) and compared with 20 nm CeO₂ and 40 nm TiO₂ nanoparticles as positive and negative control, respectively. Exposure to both Al₂O₃ nanoparticles for 24 h at 10 and 25 µg mL⁻¹ doses significantly decreased cell viability compared with control. However, the cytotoxicity of 13 and 22 nm Al₂O₃ nanoparticles had no difference at 5–25 µg mL⁻¹ dose range. The cytotoxicity of both Al₂O₃ nanoparticles were higher than negative control TiO₂ nanoparticles but lower than positive control CeO₂ nanoparticles (TiO₂ < Al₂O₃ < CeO₂). A real-time single cell imaging system was employed to study the cell membrane potential change caused by Al₂O₃ and CeO₂ nanoparticles using a membrane potential sensitive fluorescent probe DiBAC₄(3). Exposure to the 13 nm Al₂O₃ nanoparticles resulted in more significant depolarization than the 30 nm Al₂O₃ particles. On the other hand, the 20 nm CeO₂ particles, the most toxic, caused less significant depolarization than both the 13 and 22 nm Al₂O₃. Factors such as exposure duration, surface chemistry, and other mechanisms may contribute differently between cytotoxicity and membrane depolarization.

Keywords: cytotoxicity; aluminum oxide (Al₂O₃); nanoparticles; lung cancer cells (A549); depolarization; cell imaging

Introduction

Nanomaterials are defined by the US National Nanotechnology Initiative as materials that have at least one dimension in the 1–100 nm range. In the past decade, nanotechnology has become one of the leading technologies (Stix 2001). Consequently, public concern about the environmental and health effects of nanomaterials is growing rapidly. Humans may be exposed to nanoparticles via several possible routes, including inhalation, dermal absorption, and gastrointestinal tract absorption. Due to their unique properties such as small size and corresponding large specific surface area, nanomaterials may impose

*Corresponding author. Email: yinfa@umr.edu

different biological effects from their micro-scale material counterparts (Oberdorster, Oberdorster, and Oberdorster 2005; Nel et al. 2006). However, to date, toxicological and environmental effects of nanomaterials remain largely unknown.

As one of the widely studied and used nanomaterials, aluminum oxide (Al_2O_3) nanoparticles have been applied in catalysis (Jodin et al. 2006), structural ceramics for reinforcements (Bertsch, Jiguët, and Renaud 2004), polymer modification (Cho, Joshi, and Sun 2006), functionalization of textiles (Textor, Schroeter, and Schollmeyer 2006), heat transfer fluids (You, Kim, and Kim 2003), and waste water treatment (Pacheco et al. 2006). In addition, Al_2O_3 nanoparticles have shown wide biological applications in biosensors (Li et al. 2001), biofiltration, drug delivery (Popat et al. 2004), and antigen delivery for immunization purposes (Frey et al. 1999). Thus, the environmental and health impact of Al_2O_3 nanoparticles is of great interest.

The *in vitro* and *in vivo* toxicity of Al_2O_3 particles has been investigated in several studies. For instance, ceramic Al_2O_3 particles (1.3 μm , 2.4 μm) can induce significant cytotoxicity and cytokine release in macrophage cells (Catelas et al. 1998, 1999). Rollin, Theodorou, and Kilroe-Smith (1991) studied the deposition of aluminum in tissues of rabbits exposed to inhalation of low concentration of Al_2O_3 dust; they suggested an extensive study to determine a more correct TLV (threshold limit value) and health based permissible concentration for occupational exposure to aluminum. Olivier et al. (2003) investigated the cytotoxicity of 0.43 and 2.81 μm Al_2O_3 particles toward macrophage and fibroblast cells, and the results demonstrated that incubation with both sizes of Al_2O_3 significantly decreased cell numbers in a particle concentration-dependent manner. However, these previous studies only focused on micro-scale Al_2O_3 particles. To date, mechanisms of the cytotoxicity induced by Al_2O_3 nanoparticles have not been reported. Depolarization is a decrease in the absolute value of a cell's membrane potential; that is, changes in membrane voltage in which the membrane potential becomes less negative indicate depolarization. In cell function, the potential across the membrane plays an important role by controlling ion fluxes across the cell membrane, signal transduction as well as osmotic balance of the cell. Studies have shown that depolarization appears to be an early sign of cell damage because of the cytotoxic activity of toxins (Ordonez et al. 1990; Radosevic et al. 1993).

In this study, we used DiBAC₄(3) as the indicator of membrane potential. DiBAC₄(3) is an anionic probe whose distribution across the cell membrane depends on membrane potential. When depolarization occurs, more dye enters the cells, resulting in an increase of fluorescence inside the cell.

The first objective of this study was to evaluate the cytotoxicity of Al_2O_3 nanoparticles (13 nm, 22 nm) in human bronchoalveolar carcinoma-derived cells (A549). This cell line has been widely used in *in vitro* cytotoxicity studies (Huang, Khor, and Lim 2004; Upadhyay 2003). Twenty nanometer CeO_2 nanoparticles were used as a positive control because our previous study had showed that CeO_2 nanoparticles induce significant cytotoxicity at 5–25 $\mu\text{g mL}^{-1}$ dose range (Lin et al. 2006b). Forty nanometer TiO_2 nanoparticles were selected as negative control because of its well-known no or low cytotoxicity (Lee, Trochimowicz, and Reinhardt 1985; Hussain et al. 2005). In the present study, particles were dispersed in the cell culture medium and diluted to 25, 10, and 5 $\mu\text{g mL}^{-1}$ doses and then immediately applied to cells. Cytotoxicity was measured by determining cell viability with the sulforhodamine B (SRB) method (Skehan 1990). The second objective of this study was to investigate a possible depolarization mechanism caused by nanoparticles. To accomplish this, we used a single molecule and single cell

imaging system (SMIS) with freshly-suspended nanoparticles in a free solution to monitor the initial interactions between nanoparticles and cells (Ma et al. 2001; Gai et al. 2005).

Experimental

Nanoparticles

Cerium oxide (CeO_2 , 20 nm) and aluminum oxide (Al_2O_3 , 13 nm, 22 nm) were synthesized with the room temperature homogeneous nucleation method (Zhou, Anderson, and Huebner 2002). Titanium oxide (TiO_2 , 40 nm) was purchased from NanoScale Materials, Inc. (Manhattan, KS, USA). Particle size and distribution were analyzed by a Philips EM430 transmission electron microscopy (TEM) (Philips Electron Optics, Eindhoven, Holland). Crystal structures were characterized by a Scintag XDS 2000 diffractometer (Scintag, Inc., Cupertino, CA, USA). The surface area of the particles was determined by a Quantachrome Autosorb 1-C (Boynton, FL, USA). The characterization results are shown in Table 1.

Due to their nanoscale size and surface properties, nanoparticles tend to aggregate or precipitate in suspensions. In the present experiment, no dispersing agent such as a surfactant was used to improve the dispersion. As a result, the cells were exposed to and interacted with aggregated particles instead of individual particles. To understand the existing form of nanoparticles, the hydrodynamic size (aggregation size) of these four nanoparticles in cell culture medium was determined by dynamic light scattering using a Nanotrak NPA250 (Microtrac, North Largo, FL, USA).

In the cytotoxicity study (SRB assay), each stock suspension of nanoparticles was freshly prepared in the cell culture medium and dispersed using a sonication bath (FS-60H, 130 W, 20 kHz, Fisher Scientific, Pittsburg, PA, USA) for 5 min. Then the suspension was diluted to three doses (5, 10, and $25 \mu\text{g mL}^{-1}$) and immediately applied to the A549 cells. The selection of $5\text{--}25 \mu\text{g mL}^{-1}$ dose range was based on our preliminary dose response experiments of Al_2O_3 nanoparticles (13 nm, 22 nm) at $1\text{--}200 \mu\text{g mL}^{-1}$ dose range for 24 h exposure time (data not shown). The doses higher than $25 \mu\text{g mL}^{-1}$ caused severe precipitation during the exposure time, so the doses higher than $25 \mu\text{g mL}^{-1}$ were not used and doses lower than $5 \mu\text{g mL}^{-1}$ showed no cytotoxicity in A549 cells.

The nanoparticle suspensions in cell imaging buffer (see Chemicals section) for the cell imaging experiments were freshly prepared and diluted to $25 \mu\text{g mL}^{-1}$, which was the highest dose in the cytotoxicity study.

Table 1. Characterization of Al_2O_3 (13 nm, 22 nm), 20 nm CeO_2 and 40 nm TiO_2 . The particle size, surface area, crystalline structure, and hydrodynamic size were determined by TEM, BET surface area analyzer, X-Ray Diffraction (XRD), and dynamic light scattering spectroscopy, respectively.

Particles	Size and distribution nm (mean \pm SD)	Surface area (m^2/g)	Crystalline structure	Hydrodynamic size in culture medium, nm (mean \pm SD)
13 nm Al_2O_3	13 ± 2	126.9	Crystal	143 ± 57
22 nm Al_2O_3	22 ± 4	128.5	Crystal	157 ± 60
20 nm CeO_2	20 ± 3	44.0	Crystal	185 ± 61
40 nm TiO_2	40 ± 8	560.4	Amorphous	150 ± 56

Chemicals

Fetal bovine serum was purchased from the American Type Culture Collection (ATCC) (Manassas, VA, USA). Ham's F-12 medium with l-glutamine, KCl, Na₂HPO₄, and NaHCO₃ was purchased from Fisher Scientific (Pittsburg, PA, USA). Penicillin-streptomycin, trichloroacetic acid (TCA), acetic acid, FeSO₄, MgSO₄, and ZnSO₄ were purchased from Sigma (Saint Louis, MO, USA). The CaCl₂, NaCl, and D-glucose were obtained from Aldrich (Milwaukee, WI, USA). Sulforhodamine B (SRB) was bought from ICN Biomedicals (Irvine, CA, USA). The fluorescent marker bis-(1,3-dibutylbarbituric acid)trimethine oxonol (DiBAC₄(3)) was purchased from Molecular Probes (Eugene, OR, USA). Ultrapure DI-water was prepared using a Milli-Q system (Millipore, Bedford, MA, USA).

The buffer used for cell imaging experiments contained CaCl₂, NaCl, d-glucose, FeSO₄, MgSO₄, ZnSO₄, KCl, Na₂HPO₄, and NaHCO₃ at the same concentrations found in Ham's F-12 culture medium. The buffer was adjusted to pH 7.2 and filtered using a sterile 0.2 μm polyethersulfone filter. The dye DiBAC₄(3) was added to the imaging buffer to a concentration of 1.5 μM immediately before each experiment.

Cell culture

The human bronchoalveolar carcinoma-derived cell line, A549, was purchased from ATCC (Manassas, VA, USA). Cells were maintained in Ham's F-12 medium supplemented with 10% fetal bovine serum and 100 units mL⁻¹ penicillin, 100 μg mL⁻¹ streptomycin, and grown at 37°C in a 5% CO₂ humidified environment. For the SRB assay, A549 cells were plated into a 24-well plate at a density of 2.0 × 10⁴ cells per well in 1.0 mL culture medium and allowed to attach for 48 h. For the single cell imaging experiment with SMIS, the cells were cultured on a sterile No. 1.5, 22 mm square glass cover plate.

Assessment of cytotoxicity

After the exposure of cells to nanoparticles, the medium was removed and the number of cells in each well was determined using the sulforhodamine B (SRB) assay. Briefly, cells were fixed with 500 μL of cold 10% trichloroacetic acid (TCA) for 1 h at 4°C. The TCA solution was then discarded, and the cells were washed three times with distilled water followed by drying completely in a fume hood. Five hundred microliters of 0.2% sulforhodamine B in 1% acetic acid were added to each well to stain the cells for 30 min at room temperature. The staining solution was discarded, and the cells were washed with 1% acetic acid to eliminate excess dye. After complete drying, the dye in each well was solubilized in 300 μL of cold 10 mM Tris buffer (pH 10.5). One hundred microliters of dye solution were transferred into a 96-well plate and absorbance was measured at 550 nm using a microplate reader (FLOURstar, BMG Labtechnologies, Durham, NC, USA).

Single cell imaging assembly

A high purity glass cover plate with cells cultured on one side was used in the study of cell-nanoparticle interactions. The plate was placed on the hypotenuse face of a right-angle fused-silica prism (Melles Griot, Irvine, CA; Prism UVGSFS, A = B = C = 2.54 cm) with the cultured cells facing down towards the prism surface. Before each set of experiments, the prism surface was washed with approximately 300 μL of 1.0 M HCl and approximately 500 μL of ultra pure water. The distance between the cell glass plate and prism surface was fixed at 127 μm using two PTFE film strips under opposite edges of the plate. The plate

was strapped firmly in place to prevent it from shifting or floating. Sample suspensions were first introduced into the channel using hydrostatic pressure at one open edge of the resulting 15 mm channel, while excess sample suspension was removed with a wick at the opposite edge. A 3 mL reservoir coupled to polytetrafluoroethylene (PTFE) tubing and a 75 μm inner diameter fused silica capillary delivered a continual flow of sample suspension at a rate of 3.5 $\mu\text{L min}^{-1}$ of the 25 $\mu\text{g mL}^{-1}$ nanoparticle suspension. A continual flow design was used because of the very small volume of sample suspension contained in the 15 mm channel. While cells in the cytotoxicity assessment experiment were exposed to a nanoparticle suspension in the milliliter volume range, the nanoparticle suspension volume in the imaging channel was approximately 40–50 μL . The difference in volumes meant that the cells exposed in the cytotoxicity experiment experienced contact with a “bulk suspension,” and therefore a nanoparticle number limited only by the rate of diffusion of the particles within that suspension. However, it was possible that cells exposed in the 15 mm channel would bind nanoparticles, thereby decreasing the number and concentration of nanoparticles in the extracellular environment. The slow yet continual stream of sample suspension assured that the concentration of nanoparticles in the small experiment chamber was constantly refreshed, without introducing a very large flow that might influence experimental results. The experimental setup is shown in Figure 1.

Cell labeling for single cell imaging

The fluorescent marker DiBAC₄(3) was used to monitor the cells, as its fluorescence intensity is membrane potential-dependent (Laskey et al. 1992; Cornfield 1994). Each glass plate with adhering cultured cells was individually incubated at 37°C in fresh dye-spiked imaging buffer for 30 min. The glass plate was then removed, the side with cells was rinsed with 0.5 mL cell imaging buffer, and the plain glass side was carefully washed with ultra-pure water, dried, and prepared for the oil immersion objective with a drop of immersion oil. The glass was held at such an angle so that the ultra-pure water did not come into contact with the cells.

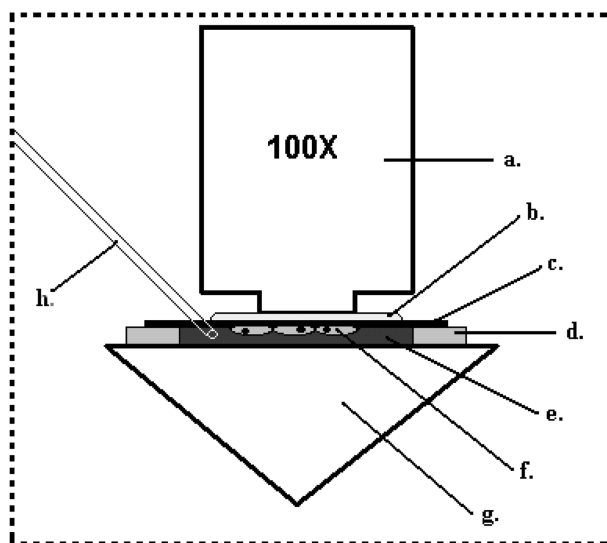


Figure 1. Sample introduction system for single cell imaging: (a) Objective; (b) Immersion oil; (c) Glass cover plate; (d) PTFE support; (e) Buffer; (f) Cells; (g) Prism; (h) Capillary.

Equipment setup

The experimental setup for this study represents a minor modification of the data acquisition system used in our previous experiments (Ma et al. 2001; Gai et al. 2005) and is shown in Figure 2. An Intensified Charge-Coupled Device (ICCD) camera (Princeton Instruments, Trenton, NJ, USA) was mounted on top of an Olympus upright microscope. The digitization rate of the camera was 5 MHz (12 bits), the controller gain was set at 70 and the camera was kept at -20°C . The camera was operated in the internal synchronization mode and in the frame-transfer mode. The excitation source was an argon ion laser at 488 nm (Spectral Physics, Mountain View, CA, USA). Extraneous light and plasma lines from the laser were eliminated prior to its entry into the observation region with the aid of an equilateral dispersing prism, optical pinholes, and a 488 nm bandpass filter. The laser beam was passed through the right angle prism at an angle of 50° relative to the normal of the glass plate surface. At this angle, the laser light was totally reflected from the top surface of the glass plate to prevent scattered light from reaching the camera. A 488 nm holographic notch filter (Kaiser Optical, Ann Arbor, MI; HNFP) with optical density of >6 and a 514–533 nm bandpass filter (Omega Optical, Brattleboro, VT; No. XF3003) were placed between the objective and the ICCD. An Olympus 100 \times , 1.3 NA UPlanFl oil microscope objective was used to collect the fluorescence from the labeled cells. Imaging data were collected using Winview/32 software (Princeton Instruments, Trenton, NJ, USA).

The imaging data were analyzed as follows: for each sample, an image data file consisting of 25 video frames was collected every 5 min. Within each imaging file, a single cell was selected. Coordinates for the fluorescence signal at the brightest part of the cell were used to select that region of interest for numerical data analysis. The minimum size of this region of interest was typically 10×15 pixels in size. The software calculated the average fluorescence signal in the region of interest. This average was calculated for all 25 frames of each data file, and these 25 averages were averaged in order to arrive at a single value for the fluorescence intensity of the cell's response in that imaging data file.

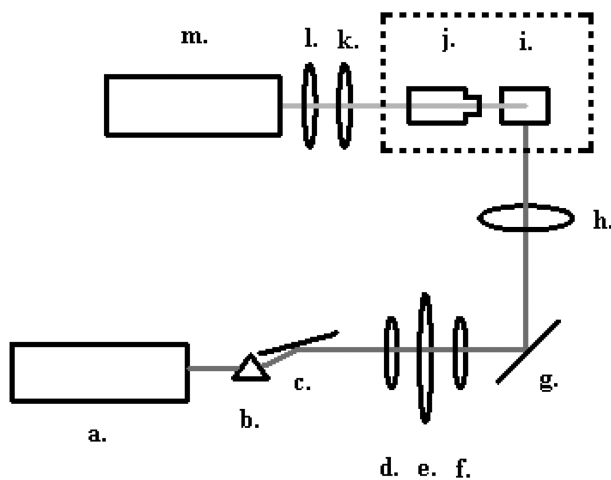


Figure 2. Optical setup for single cell imaging: (a) Laser; (b) Prism; (c) Mirror; (d) Pinhole; (e) Shutter; (f) Pinhole; (g) Mirror; (h) 488 Bandpass filter; (i) Sample and prism; (j) Microscope objective; (k) 488 notch filter; (l) Emission bandpass filter; (m) Camera.

The same regions of interest were used for all imaging data files of a given sample, to ensure that the same specific region of the same specific cell was measured every 5 min. The process was repeated to collect cell responses from multiple cells within each sample. Imaging data file examination showed that the cell response in the dimmer regions of the cell mirrored the trend in the bright regions, so the bright fluorescence regions were chosen arbitrarily for analysis. In addition, it was determined that within the 25 frames of an imaging data file, no great trend was typically visible in cell response from frame 1 to frame 25. For this reason, the 25 data frames were averaged together. Multiple cells were investigated for all samples, though cell response within each sample was very similar from cell to cell. Since cells in the same sample under the same conditions may yield slightly different levels of fluorescence intensity (Brauner, Hulser, and Strasser 1984), the percent change in fluorescence was compared over the course of the experiment. Finally, in order to account for environmental changes such as laser power fluctuations, a sample region containing no cells was analyzed and averaged, and then subtracted from the cellular fluorescence signal prior to the calculation of percent intensity change.

Statistical analysis

In SRB assay, data were expressed as the mean \pm SD from three independent experiments. One-tailed unpaired Student's *t*-test was used for significance testing, using a *p*-value of 0.05. In cell imaging experiment, the same *t*-test was performed to determine if the relative fluorescence signal of the cell imaging data were significantly different from control samples.

Results

Particle characterization

The results from the characterization of Al₂O₃, CeO₂, and TiO₂ nanoparticles were summarized in Table 1. The mean size and distribution of two sizes of Al₂O₃ nanoparticles were 13 \pm 2 and 22 \pm 4 nm. The surface areas of these two sizes of Al₂O₃ by BET measurement were 126.9 and 128.5 m² g⁻¹, respectively. Thirteen and 22 nm Al₂O₃ nanoparticles demonstrated almost the same specific surface area, probably due to their aggregation. The XRD analysis clearly showed the crystalline structure of both Al₂O₃ nanoparticles.

The hydrodynamic size of nanoparticles measured by a dynamic light scattering method indicates the extent of particle aggregation in culture medium (Table 1). The hydrodynamic sizes of 13 and 22 nm Al₂O₃ nanoparticles in medium were 143 \pm 57 and 157 \pm 60 nm (*p* > 0.05), respectively, indicating that aggregation occurred. The hydrodynamic sizes of CeO₂ and TiO₂ nanoparticles were 185 \pm 61 and 150 \pm 56 nm, respectively.

The cytotoxicity of Al₂O₃ (13 nm, 22 nm) nanoparticles

After A549 cells were exposed to Al₂O₃ nanoparticles (13 nm, 22 nm) at 5, 10, and 25 μ g mL⁻¹ for 24 h, cell viability decreased as a function of dose levels (Figure 3). A dose of 5 μ g mL⁻¹ of 13 nm Al₂O₃ did not affect cell viability, while cell viability decreased significantly to 86.0 and 82.8% at 10 and 25 μ g mL⁻¹ doses, respectively (*p*'s < 0.05), in comparison with the control group. The dose response curve of the 22 nm Al₂O₃ particles showed a similar trend; 10 and 25 μ g mL⁻¹ doses decreased the cell viability

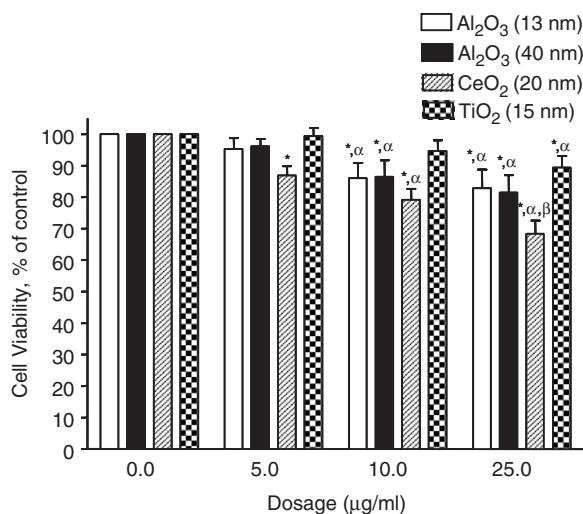


Figure 3. Viability of A549 cells after 24 h exposure to 5, 10, or 25 $\mu\text{g mL}^{-1}$ of Al_2O_3 (13 nm, 22 nm), CeO_2 (20 nm), and TiO_2 (40 nm). CeO_2 and TiO_2 were used as positive and negative control, respectively. Values are mean \pm SD from three independent experiments. Triplicates of each treatment group were used in each independent experiment. Significance indicated by: * $p < 0.05$ vs. control cells, $^{\alpha}p < 0.05$ vs. cells exposed to 5 $\mu\text{g mL}^{-1}$ dose, $^{\beta}p < 0.05$ vs. cells exposed to 10 $\mu\text{g mL}^{-1}$ dose.

significantly to 86.4 and 81.4%, respectively (p 's < 0.05). Interestingly, the cytotoxicity of both Al_2O_3 particles had no significant difference from one another at 5–25 $\mu\text{g mL}^{-1}$.

Twenty nanometer CeO_2 nanoparticles and 40 nm TiO_2 nanoparticles were used as the positive control and negative control, respectively, to evaluate the relative cytotoxicity of Al_2O_3 nanoparticles (Figure 3). The cell viability of the groups exposed to 5, 10, and 25 $\mu\text{g mL}^{-1}$ CeO_2 particles decreased significantly to 86.8, 79.1, and 68.3%, respectively, compared to the control group (p 's < 0.05). However, only 25 $\mu\text{g mL}^{-1}$ dose of 40 nm TiO_2 nanoparticles significantly decreased cell viability to 89.3% ($p < 0.05$). The cytotoxicity order of these particles is: 20 nm $\text{CeO}_2 > 13$ nm $\text{Al}_2\text{O}_3 = 22$ nm $\text{Al}_2\text{O}_3 > 40$ nm TiO_2 nanoparticles.

Time course and dose-dependent cytotoxicity of 13 nm Al_2O_3 nanoparticles

Due to the similar cytotoxicity, only 13 nm Al_2O_3 nanoparticles was used in the subsequent time course cytotoxicity study. A549 cells were exposed to Al_2O_3 at 5, 15, and 25 $\mu\text{g mL}^{-1}$ dose levels for 6, 12, and 24 h. No doses after 6 h exposure showed significant different of cell viability compared with control group (Figure 4). However, the 25 $\mu\text{g mL}^{-1}$ dose showed significant cytotoxicity after 12 h exposure. After 24 h exposure, cell viability decreased further to 95.3, 86.0, and 82.8%, compared to the control, indicating the time-dependent cytotoxicity of Al_2O_3 nanoparticles.

Single cell imaging to study the interaction of nanoparticles with cells

To investigate the initial interactions of nanoparticles with the cells, we conducted a single cell imaging experiment using a SMIS. The nanoparticles chosen for investigation were 20 nm CeO_2 , 13 nm Al_2O_3 , and 22 nm Al_2O_3 , because they showed greater cytotoxicity in

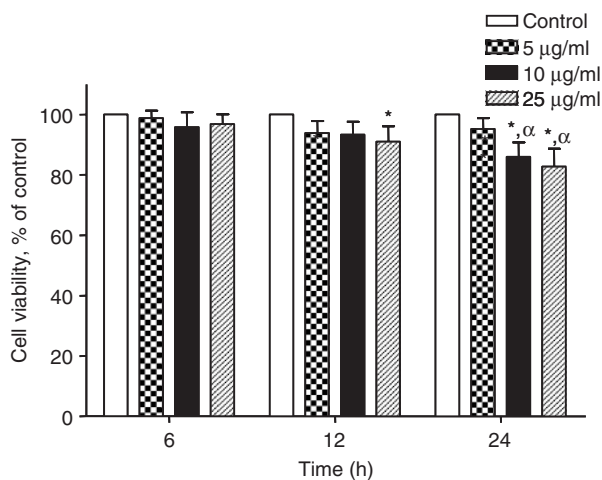


Figure 4. Viability of A549 cells after 6, 12, and 24 h exposure to 5, 10, or 25 $\mu\text{g mL}^{-1}$ of 13 nm Al_2O_3 nanoparticles. Values are mean \pm SD from three independent experiments. Triplicates of each treatment group were used in each independent experiment. Significance indicated by: * $p < 0.05$ vs. control cells, $^{\alpha}p < 0.05$ vs. cells exposed to 5 $\mu\text{g mL}^{-1}$ dose.

the dose response experiment. Cells were exposed to the same concentration (25 $\mu\text{g mL}^{-1}$) of nanoparticles, while the environment for control cells was imaging buffer. The concentration of nanoparticles chosen was stable for at least 1.5 h in this particular SMIS system. The cells were first labeled with the fluorescent membrane potential marker DiBAC₄(3). An increase in fluorescence signal is an indication that the potential across the cell membrane is less negative than the membrane potential in healthy control cells. The fluorescence intensity of the control cells changed little over the course of 1 h. In contrast, cells exposed to the various nanoparticles showed a distinct increase in fluorescence intensity over the same period of time (Figure 5). Specifically, at the end of one hour, 13 nm Al_2O_3 -treated cells showed an average signal increase of 86%, which was the greatest signal change seen during the experiment. Cells dosed with 22 nm Al_2O_3 showed an average signal increase of 45%, while the 20 nm CeO_2 -treated cells showed the least degree of signal increase, 37%. The control exhibited a relatively stable fluorescence signal, with the maximum average signal change being observed at 14%. Nanoparticle-exposed samples were statistically different from the average control signal at different times. The 22 nm Al_2O_3 -treated cells showed a significant difference from the control by 10 min ($p < 0.05$, $N = 19$), yet the percent change in signal leveled out by approximately 30 min. The 13 nm Al_2O_3 -treated cells showed a significant increase in signal by 15 min ($p < 0.05$, $N = 12$), and 20 nm CeO_2 -treated cells by 55 min ($p < 0.05$, $N = 7$). The signal change in the Al_2O_3 -treated cells was visibly evident. Cell morphology remained generally unchanged throughout the experiment.

Discussion

Cytotoxicity of Al_2O_3 nanoparticle

The purpose of this study was to compare the potential cytotoxicity of two sizes of Al_2O_3 nanoparticles (13 nm, 22 nm) in cultured human bronchoalveolar carcinoma-derived cells. To date there are very few studies investigating the toxic effects and mechanisms of

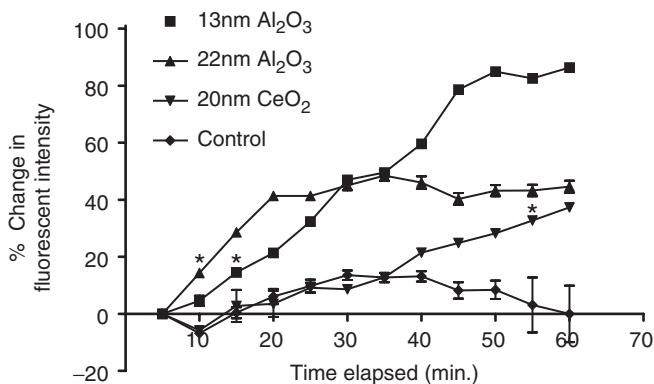


Figure 5. Averaged percent change in fluorescence intensity for Al₂O₃ and CeO₂ nanoparticles, and control. Data were expressed as mean \pm coefficient of variation. The coefficient of variation is calculated by multiplying the standard deviation by 100 and dividing by the average. Nanoparticle data with an asterisk (*) above them designate the first point in each respective nanoparticle data series to be significantly different from the controls. This significance for 13 nm Al₂O₃ ($N=12$), 22 nm Al₂O₃ ($N=19$) and 20 nm CeO₂ ($N=7$) was calculated using Student's *t*-test ($p < 0.05$).

Al₂O₃ nanoparticles. Our results showed that the both 13 nm Al₂O₃ nanoparticles and 22 nm Al₂O₃ nanoparticles induced significant cytotoxicity at the levels of 5–25 $\mu\text{g mL}^{-1}$. In addition, the cytotoxicity of 13 nm Al₂O₃ nanoparticles at the dose levels of 5–25 $\mu\text{g mL}^{-1}$ for 6, 12, and 24 h exposure showed that the cytotoxicity is dose- and time-dependent.

To determine whether the cytotoxicity of Al₂O₃ particles (13 nm *versus* 22 nm) is size-dependent was one of our objectives. It is generally perceived that smaller particles cause greater toxicity because of their relatively larger specific surface area. For instance, in a previous study using titanium of diameters 3, 10, 50, and 150 μm and titanium oxide of diameters 3 μm , 50, and 500 nm, the survival rate of neutrophils decreased as the particle size decreased (Tamura et al. 2004). Brown et al. (2001) have shown the size-dependent proinflammatory effects of ultrafine polystyrene particles. However, our data showed similar cytotoxicity between 13 and 22 nm Al₂O₃ particles in the 5–25 $\mu\text{g mL}^{-1}$ dose range. This result may mainly be due to aggregation of Al₂O₃ nanoparticles in the cultured medium. Based upon the hydrodynamic size data, the 13 and 22 nm Al₂O₃ particles aggregated to form the similar hydrodynamic sizes of 143 ± 57 and 157 ± 60 nm, respectively. The similar hydrodynamic sizes might provide an explanation as to why they showed similar cytotoxicity. Our previous study of cytotoxicity of 15 and 64 nm SiO₂ nanoparticles also showed the similar hydrodynamic size and cytotoxicity (Lin et al. 2006a). Because metal oxide nanoparticles, such as Al₂O₃, TiO₂, and CeO₂ tend to aggregate in cell culture medium and the aggregation size (hydrodynamic size) is quite different from its original particle size, the aggregation size of nanoparticles should also be considered in an *in vitro* study. Because of the complexity and diverse properties of particles, such as composition, size, shape, aggregation, surface activities, surface treatment, and crystallinity, a complete evaluation of the effects of various particle properties is warranted (Oberdorster, Oberdorster, and Oberdorster 2005).

Single cell imaging and the interaction of nanoparticles with cells

To investigate possible initial mechanisms of toxicity, we studied changes in cell membrane potential by monitoring the fluorescence intensity of the anionic cell membrane marker DiBAC₄(3). This marker has been widely used for investigating cell membrane behavior while cells are under environmental stress or other conditions (Xie and Zhuang 2001; Wolff, Fuks, and Chatelain 2003; Allen and Kirk 2004). When depolarization of the cell membrane occurs, the transmembrane dye equilibrium shifts, causing the dye to migrate inside the cell from the extracellular environment. The reverse is also true; hyperpolarization causes the observed fluorescence signal to decrease. In this study, the increase in fluorescence signal indicated depolarization of the cell membrane after the cells were exposed to Al₂O₃ and CeO₂ nanoparticles. Such a condition could be caused by a number of pathways, including a protein-mediated influx of a specific cation(s), expulsion of a specific anion(s), or by physical breaches of the membrane. Under normal conditions, the potential across the cell membrane is maintained by the active transport of cations through the lipid bilayer (Widmaier, Raff and Strang 2004). Since the concentrations of ions such as Cl⁻, K⁺, Ca²⁺, and Na⁺ within the cell help regulate physiological pathways, a change in the concentration of each can activate a variety of mechanisms within the cell (Becker, Kleinsmith, and Hardin 2000). This includes even the triggering of apoptosis, as is the case with Ca²⁺ (Orrenius, Zhivotovsky, and Nicotera 2003). Further research is necessary to further understand the exact pathway(s) by which the membrane potential is changed.

Exposure to the nanoparticles tested in the cell imaging experiment caused a distinct increase in the fluorescence intensity of the DBAC₄ dye in the cells (Figure 5). Of the three kinds of particles studied, the 13 nm Al₂O₃ nanoparticles appeared to have the greatest influence upon the cells. Moreover, the effect was time-dependent. Oscillation of the signal was observed in control cells, but the signal did not increase sharply. An ANOVA of the control data revealed that the control groups were not significantly different from one another ($p > 0.05$). The 13 nm Al₂O₃ caused the most membrane depolarization during the measured exposure time, followed by 22 nm Al₂O₃. Because the Al₂O₃ particles disrupted the membrane potential more than the CeO₂ particles in the imaging experiment, the data from imaging the cell membrane potential change did not agree with the Al₂O₃ nanoparticle cytotoxicity data.

In the cytotoxicity study, the 20 nm CeO₂ showed the greatest cytotoxicity. Different factors may contribute to this apparent discrepancy. First, the exposure time during the imaging experiment (60 min) was very short compared to the 24 h exposure in the cytotoxicity experiment. Thus, any changes observed during the imaging experiment represent only the *initial* effects of nanoparticles upon the cells. Cellular environmental conditions limited the length of the imaging study, as neither temperature nor atmospheric gas concentrations could be regulated. Second, it is reasonable to propose that the Al₂O₃ nanoparticles may exhibit faster kinetics than CeO₂ nanoparticles when moving through the solution and interacting with the cells, due to the lower density of Al₂O₃ nanoparticles. Third, CeO₂ nanoparticles may produce toxicity via mechanisms that do not involve disrupting the membrane potential. For example, our previous study has shown the cytotoxicity of CeO₂ nanoparticles was related to an oxidative stress mechanism and lipid peroxidation (Lin et al. 2006b). Fourth, since the chemical surfaces of the CeO₂ and Al₂O₃ nanoparticles are different, they may interact with the membrane differently. The metal atoms on the surface of the two kinds of metal oxide nanoparticles are different in their size, charge (and charge density), valence electrons and valence electron orbital arrangements. These several factors may cause the difference in reaction time with the

cell membrane, as well as affect the number of nanoparticles interacting with the membrane. The presence of such differentiating factors would eventually cause a difference in the levels of cytotoxicity. These are areas meriting further research.

Conclusion

We have demonstrated that 13 and 22 nm Al_2O_3 nanoparticles significantly reduce cell viability in a dose- and time-dependent manner in bronchoalveolar carcinoma-derived cells at 5–25 $\mu\text{g mL}^{-1}$ doses. Both Al_2O_3 particles showed similar cytotoxicity at a 5–25 $\mu\text{g mL}^{-1}$ doses range after 24 h exposure; this may be due to their similar aggregation size in cell culture medium. The real-time imaging study clearly indicated that cell membrane depolarization induced by two sizes of Al_2O_3 and CeO_2 nanoparticles may be one of the initial mechanisms of action for nanoparticle cytotoxicity.

Acknowledgements

We thank the Department of Chemistry, the Department of Biological Sciences, and the Environmental Research Center for Emerging Contaminants at the University of Missouri-Rolla for financial support. Thanks also go to Robert S. Aronstam for technical editing.

References

- Allen, R.J., and K. Kirk. 2004. The membrane potential of the intraerythrocytic malaria parasite *Plasmodium falciparum*. *Journal of Biological Chemistry* 279: 11264–72.
- Becker, W.M., L.J. Kleinsmith and J. Hardin. 2000. *The World of the Cell*, p. 212, San Francisco, CA, USA: Benjamin/Cummings.
- Bertsch, A., S. Jiguet, and P. Renaud. 2004. Microfabrication of ceramic components by microstereolithography. *Journal of Micromechanics and Microengineering* 14: 197–203.
- Brauner, T., D.F. Hulser, and R.J. Strasser. 1984. Comparative measurements of membrane potentials with microelectrodes and voltage-sensitive dyes. *Biochimica et Biophysica acta* 771: 208–16.
- Brown, D.M., M.R. Wilson, W. MacNee, V. Stone, and K. Donaldson. 2001. Size-dependent proinflammatory effects of ultrafine polystyrene particles: A role for surface area and oxidative stress in the enhanced activity of ultrafines. *Toxicology and Applied Pharmacology* 175: 191–9.
- Catelas, I., O.L. Huk, A. Petit, D.J. Zukor, R. Marchand, and L. Yahia. 1998. Flow cytometric analysis of macrophage response to ceramic and polyethylene particles: Effects of size, concentration, and composition. *Journal of Biomedical Materials Research* 41: 600–7.
- Catelas, I., A. Petit, R. Marchand, D.J. Zukor, L. Yahia, and O.L. Huk. 1999. Cytotoxicity and macrophage cytokine release induced by ceramic and polyethylene particles *in vitro*. *Journal of Bone and Joint Surgery – British Volume* 81: 516–21.
- Cho, J., M.S. Joshi, and C.T. Sun. 2006. Effect of inclusion size on mechanical properties of polymeric composites with micro and nano particles. *Composites Science and Technology* 66: 1941–52.
- Cornfield, D.N., T. Stevens, I.F. McMurtry, S.H. Abman, and D.M. Rodman. 1994. Acute hypoxia causes membrane depolarization and calcium influx in fetal pulmonary artery smooth muscle cells. *American Journal of Physiology* 266: L469–L75.
- Frey, A., N. Mantis, P.A. Kozlowski, A.J. Quayle, A. Bajardi, J.J. Perdomo, F.A. Robey, and M.R. Neutra. 1999. Immunization of mice with peptomers covalently coupled to aluminum oxide nanoparticles. *Vaccine* 17: 3007–19.

- Gai, H., Y. Li, Z. Silber-Li, Y. Ma., and B. Lin. 2005. Simultaneous measurements of the flow velocities in a microchannel by wide/evanescent field illuminations with particle/single molecules. *Lab on a Chip* 5: 443–9.
- Huang, M., E. Khor, and L.Y. Lim. 2004. Uptake and cytotoxicity of chitosan molecules and nanoparticles: Effects of molecular weight and degree of deacetylation. *Pharmaceutical Research* 21: 344–53.
- Hussain, S.M., K.L. Hess, J.M. Gearhart, K.T Geiss, and J.J Schlager. 2005. *In vitro* toxicity of nanoparticles in BRL 3A rat liver cells. *Toxicology In Vitro* 19: 975–83.
- Jodin, L., A.-C. Dupuis, E. Rouviere, and P. Reiss. 2006. Influence of the catalyst type on the growth of carbon nanotubes via methane chemical vapor deposition. *Journal of Physical Chemistry B* 110: 7328–33.
- Laskey, R.E., D.J. Adams, M. Cannell, and C. van Breemen. 1992. Calcium entry-dependent oscillations of cytoplasmic calcium concentration in cultured endothelial cell monolayers. *Proceedings of the National Academy of Sciences of the United States of America* 89: 1690–4.
- Lee, K.P., H.J. Trochimowicz, and C.F. Reinhardt. 1985. Pulmonary response of rats exposed to titanium dioxide (TiO₂) by inhalation for two years. *Toxicology and Applied Pharmacology* 79: 179–92.
- Li, J., Y. Wang, J. Wang, M. Harvey, D.A. Atwood and L.G. Bachas. 2001. *Immobilization of phosphorylated proteins on alumina nanoparticles: Toward nanosize biosensors*. 221st ACS National Meeting, Vol. 1–5, ANYL-081. San Diego, CA, United States: American Chemical Society.
- Lin, W., Y.-W. Huang, X.-D. Zhou and Y. Ma. 2006a. *In vitro* toxicity of silica nanoparticles in human lung cancer cells. *Toxicology and Applied Pharmacology*, 217: 252–259.
- Lin, W., Y.-W. Huang, X.-D. Zhou, and Y. Ma. 2006b. Toxicity of cerium oxide nanoparticles in human lung cancer cells. *International Journal of Toxicology* 25: 1–7.
- Ma, Y., M.R. Shortreed, H. Li, W. Huang, and E.S. Yeung. 2001. Single-molecule immunoassay and DNA diagnosis. *Electrophoresis* 22: 421–6.
- Nel, A., T. Xia, L. Madler, and N. Li. 2006. Toxic potential of materials at the nanolevel. *Science* 311: 622–7.
- Oberdorster, G., E. Oberdorster, and J. Oberdorster. 2005. Nanotoxicology: An emerging discipline evolving from studies of ultrafine particles. *Environmental Health Perspectives* 113: 823–39.
- Olivier, V., J.L. Duval, M. Hindie, P. Pouletaut, and M.D. Nagel. 2003. Comparative particle-induced cytotoxicity toward macrophages and fibroblasts. *Cell Biology and Toxicology* 19: 145–59.
- Ordonez, J.V., H.M. Rubinstein, and J.W. Burnett. 1990. Flow cytometric detection of jellyfish venom induced cytotoxicity. *Toxicon* 28: 863–7.
- Orrenius, S., B. Zhivotovsky, and P. Nicotera. 2003. Regulation of cell death: The calcium-apoptosis link. *Nature Review: Molecular Cell Biology* 4: 552–65.
- Pacheco, S., M. Medina, F. Valencia, and J. Tapia. 2006. Removal of inorganic mercury from polluted water using structured nanoparticles. *Journal of Environmental Engineering* 132: 342–9.
- Popat, K.C., G. Mor, C.A. Grimes, and T.A. Desai. 2004. Surface modification of nanoporous alumina surfaces with poly(ethylene glycol). *Langmuir* 20: 8035–41.
- Radosevic, K., T.C. Schut, M. van Graft, B.G. de Grooth, and J. Greve. 1993. A flow cytometric study of the membrane potential of natural killer and K562 cells during the cytotoxic process. *Journal of Immunological Methods* 161: 119–28.
- Rollin, H.B., P. Theodorou, and T.A. Kilroe-Smith. 1991. Deposition of aluminium in tissues of rabbits exposed to inhalation of low concentrations of Al₂O₃ dust. *British Journal of Industrial Medicine* 48: 389–91.
- Skehan, P., R. Storeng, D. Scudiero, A. Monks, J. McMahon, D. Vistica, J.T. Warren, H. Bokesch, S Kenney, and M.R. Boyd. 1990. New colorimetric cytotoxicity assay for anticancer-drug screening. *Journal of National Cancer Institute* 82: 1107–12.
- Stix, G. 2001. Little big science. Nanotechnology. *Scientific American* 285: 32–7.
- Tamura, K., N. Takashi, T. Akasaka, I.D. Roska, M. Uo, Y. Totsuka, and F. Watari. 2004. Effects of micro/nano particles size on cell function and morphology. *Key Engineering Materials* 254–256: 919–922.

- Textor, T., F. Schroeter and E. Schollmeyer. 2006. Functionalisation of textiles with nanotechnology. *Materials Research Society Symposium Proceedings*, Vol. 920, Materials Research Society, pp. 1–11.
- Upadhyay, D., V. Panduri, A. Ghio, and D.W. Kamp. 2003. Particulate matter induces alveolar epithelial cell DNA damage and apoptosis: role of free radicals and the mitochondria. *American Journal of Respiratory Cell and Molecular Biology* 29: 180–7.
- Widmaier, E.P., H. Raff, and K.T. Strang. 2004. *Human Physiology*, 160. New York: McGraw-Hill.
- Wolff, C., B. Fuks, and P. Chatelain. 2003. Comparative study of membrane potential-sensitive fluorescent probes and their use in ion channel screening assays. *Journal of Biomolecular Screening* 8: 533–43.
- Xie, Y., and Z.X. Zhuang. 2001. Chromium (VI)-induced production of reactive oxygen species, change of plasma membrane potential and dissipation of mitochondria membrane potential in Chinese hamster lung cell cultures. *Biomedical and Environmental Sciences* 14: 199–206.
- You, S.M., J.H. Kim, and K.H. Kim. 2003. Effect of nanoparticles on critical heat flux of water in pool boiling heat transfer. *Applied Physics Letters* 83: 3374–76.
- Zhou, X.D., H.U. Anderson, and W. Huebner. 2002. Room temperature homogenous nucleation synthesis and thermal stability of nanometer CeO₂ single crystals. *Applied Physics Letters* 80: 3814–16.